Liver Research 8 (2024) 282–294

Contents lists available at ScienceDirect

Liver Research

journal homepage: http://www.keaipublishing.com/en/journals/liver-research

Original Article

Single-cell and machine learning approaches uncover intrinsic immune-evasion genes in the prognosis of hepatocellular carcinoma

Jiani Wang [a, b, 1], Xiaopeng Chen [c, 1], Donghao Wu [d, 1], Changchang Jia [a], Qinghai Lian [a, *], Yuhang Pan [e, **], Jiumei Yang [f, ***]

[a] Cell-Gene Therapy Translational Medicine Research Center, The Third Affiliated Hospital of Sun Yat-sen University, Guangzhou, Guangdong, China
[b] Breast Cancer Center, The Third Affiliated Hospital of Sun Yat-sen University, Guangzhou, Guangdong, China
[c] Department of Hepatobiliary Surgery, The Third Clinical Medical College of Ningxia Medical University, Yinchuan, Ningxia, China
[d] Department of Medical Oncology, The Third Affiliated Hospital of Sun Yat-sen University, Guangzhou, Guangdong, China
[e] Department of Pathology, The Third Affiliated Hospital of Sun Yat-sen University, Guangzhou, Guangdong, China
[f] Medical Research Center, The Affiliated Guangdong Second Provincial General Hospital of Jinan University, Guangzhou, Guangdong, China

ARTICLE INFO

Article history:
Received 24 July 2024
Received in revised form
7 September 2024
Accepted 1 November 2024

Keywords:
Hepatocellular carcinoma (HCC)
Intrinsic immune-evasion genes (IIEGs)
The Cancer Genome Atlas (TCGA)
Machine learning
Single-cell analysis

ABSTRACT

Background and aims: Hepatocellular carcinoma (HCC) is a tumor of high heterogeneity and complexity, which poses significant challenges to effective treatment and patient prognosis because of its immune evasion characteristics. To address these issues, single-cell technology and machine learning methods have emerged as a promising approach to identify genes associated with immune escape in HCC. This study aimed to develop a prognostic risk score model for HCC by identifying intrinsic immune-evasion genes (IIEGs) through single-cell technology and machine learning, providing insights into immune infiltration, enhancing predictive accuracy, and facilitating the development of more effective treatment strategies.

Materials and methods: The study utilized data from The Cancer Genome Atlas database to analyze gene expression profiles and clinical data related to intrinsic immune evasion in patients with HCC. Various tools, including the Human Protein Atlas, cBioPortal, single-cell analysis, machine learning, and Kaplan-Meier plot, were used to analyze IIEGs. Functional enrichment analysis was conducted to explore potential mechanisms. In addition, the abundance of infiltrating cells in the tumor microenvironment was investigated using single-sample gene set enrichment analysis, CIBERSORT, xCELL, and tumor immunophenotype algorithms. The expression of glycosylphosphatidylinositol anchor attachment 1 (GPAA1) was examined in the clinical sample of HCC by quantitative real-time polymerase chain reaction, Western blotting, and immunohistochemical staining.

Results: Univariate Cox analysis identified 63 IIEGs associated with the prognosis of HCC. Using random forest, least absolute shrinkage and selection operator regression analysis, and support vector machine, a risk score model consisting of six IIEGs (carbamoyl-phosphate synthetase 2, aspartate transcarbamylase, and dihydroorotase (CAD), phosphatidylinositol glycan anchor biosynthesis class U (PIGU), endoplasmic reticulum membrane protein complex subunit 3 (EMC3), centrosomal protein 55 (CEP55), autophagy-related 10 (ATG10), and GPAA1) developed, which was validated using 10 pairs of HCC and adjacent non-cancerous samples. Based on the calculated median risk score, HCC samples were categorized into high- and low-risk groups. The Kaplan-Meier curve analysis showed that the high-risk group had a worse prognosis compared with the low-risk group. Time-dependent receiver operating characteristic analysis demonstrated the accurate predictive capability of the risk score model for HCC prognosis. Furthermore, immune infiltration analysis showed a positive correlation between the risk score model and 40 immune checkpoint genes as well as Th2 cells.

Conclusions: A prognostic risk score model was formulated by six IIEG signatures and showed promise in predicting the prognosis of patients diagnosed with HCC. The utilization of the IIEG risk score as a novel

* Corresponding author.
** Corresponding author.
*** Corresponding author.
E-mail addresses: lianqh5@mail.sysu.edu.cn (Qinghai Lian), panyh25@mail.sysu.edu.cn (Yuhang Pan), yangjm@gd2h.org.cn (Jiumei Yang).
[1] These authors contributed equally to this work.

https://doi.org/10.1016/j.livres.2024.11.001

prognostic index, together with its significance as a valuable biomarker for immunotherapy in HCC, provides benefit for patients with HCC in determining therapeutic strategies for clinical application.

1. Introduction

Hepatocellular carcinoma (HCC) remains a significant oncological challenge, ranking as the fourth leading cause of cancer-related deaths worldwide.[1–3] The HCC-related mortality rate is strongly correlated with the global incidence of newly diagnosed cases.[4] Chronic viral infections, particularly hepatitis B and C virus (HBV and HCV, respectively), are major contributors to a significant proportion of HCC occurrences.[5] These infections persist despite ongoing immune modulation during chronic viral inflammation. The immunomodulatory microenvironment plays a critical role in tumor progression, particularly in the context of HCC, where persistent hepatic inflammation or chronic hepatitis infection often precedes cancer development.[6–8] The composition of the tumor microenvironment (TME) plays a crucial role in the prognosis of patients with HCC, as it significantly influences clinical outcomes.[9–12] The development and progression of tumors involve immune system evasion, resulting in an ongoing battle between the cancer and the host.[13,14] Various phases of immune system evasion may exist, each manifesting with unique attributes and mechanisms that contribute to tumor progression.[1] Studies elucidated the precise mechanisms of immune evasion in HCC are still in early stages.[15] Despite recent advances in diagnosis, treatment, and management of HCC, long-term survival remains limited, particularly for patients with advanced HCC.[16] Current therapies, including sorafenib and regorafenib, offer only modest survival benefits, highlighting an urgent need for new treatment strategies. The complex interplay between the immune system and HCC progression is not yet fully understood,[17] and elucidating the mechanisms of immune evasion is crucial for developing more effective therapies.

Bioinformatics and biotechnology have achieved remarkable progresses, providing researchers with powerful tools and methods to explore the TME in greater detail. In particular, single-cell transcriptomics has allowed for a more precise examination of dynamics of different immune cells in HCC.[18] This technology facilitates the investigation of the roles of immune responses in tumor progression and immune evasion mechanisms. Concurrently, machine learning as an invaluable data-driven approach is increasingly used in the biomedical field. By training and optimizing machine learning algorithms, researchers can uncover potential biological patterns, derive new insights from vast quantities of biological data, and integrate these advanced approaches with clinical data to translate research findings into clinical practice. Using single-cell technology and machine learning methods, we aimed to formulate a prognostic risk score model for HCC by identifying intrinsic immune-evasion genes (IIEGs), providing perspectives into immune infiltration and TME, improving predictive accuracy, and facilitating the development of more effective treatment strategies.

2. Materials and methods

2.1. Ethical approval

This study complied with the 1975 Declaration of Helsinki and was approved by the Medical Ethics Committee of The Third Affiliated Hospital of Sun Yat-sen University (approval number: II2023-261-01). Written informed consent was obtained from each patient before the study.

2.2. Data acquisition and preprocessing

RNA sequencing (RNA-Seq) data were acquired from a cohort of 373 patients diagnosed with HCC and gene expression profiles from 50 normal tissues, immune system infiltration data, and relevant clinical information sourced from The Cancer Genome Atlas (TCGA) (https://portal.gdc.cancer.gov/).[19] Then, RNA-Seq data were transformed from the fragments per kilobase of transcript per million mapped reads (FPKM) format to the transcripts per million (TPM) format while preserving clinical data and RNA-Seq information. Following the acquisition and transformation of the RNA-Seq data as described, we proceeded to enrich our analysis by incorporating a comprehensive set of IIEGs. We identified a total of 182 IIEGs from previous literature (Supplemental Table 1),[20] which are known to play a pivotal role in the immune evasion mechanisms of various cancers, including HCC.

2.3. Enrichment analysis

The Kyoto Encyclopedia of Genes and Genomes (KEGG) database (https://www.genome.jp/kegg/) provides comprehensive information on genomes and biological pathways, and Gene Ontology (GO) annotation analysis is widely used for enrichment.[21] Among a total of 182 IIEGs, 63 were associated with HCC prognosis in the univariate analysis. To further investigate these 63 IIEGs, enrichment and analysis were performed using clusterProfiler, GO, and KEGG functions of R software. Furthermore, the DisGeNET database in WebGestalt, a web-based gene-set analysis tool, was used to predict diseases associated with the aforementioned 63 genes related to intrinsic immune evasion.

2.4. Protein expression analysis

Data for the HCC and normal tissues were retrieved from the Human Protein Atlas (HPA) (https://www.proteinatlas.org/), which utilizes transcriptome and proteomics to generate various protein expression maps, including tissue atlas, brain atlas, single-cell atlas, tissue cell atlas, and pathology atlas. Additionally, protein expression levels of IIEGs were analyzed using the UALCAN database (https://ualcan.path.uab.edu/), which offers insights into the expression profiles of genes across different cancer types.

2.5. Single-cell RNA-seq (scRNA-seq) analysis

The Tumor Immune Single-cell Hub (TISCH) database (http://tisch.comp-genomics.org/) was used for scRNA-seq analysis of six IIEGs in HCC.[22] We retrieved one HCC dataset, GSE140228, from this database for our study.

2.6. Mutation analysis

Gene variant analysis of HCC including amplification, mutation, and copy number variation was performed using cBioPortal (https://www.cbioportal.org/). The website provides an overview

of the genetic alterations in each IIEG, visualizing the full details of each type of mutation in individual sample.

2.7. Immune infiltration analysis

Four primary algorithms were used to determine the abundance of immune cells infiltrating the TME: single-sample gene set enrichment analysis (ssGSEA), xCELL, CIBERSORT, and tumor immunophenotype (TIP). Each algorithm considers slightly different cell types and reference gene sets for estimation. xCELL utilizes modified ssGSEA to estimate the scores of 38 immune and stromal cell types, including various subtypes of $CD8^+$ T, $CD4^+$ T, B, and dendritic cells, macrophage polarization, and other innate immune cells. CIBERSORT employs a linear support vector regression model to estimate the "relative" proportion of 22 immune cell types.[23,24] For ssGSEA, the gene set variation analysis (GSVA) package was used to assess the infiltration of 24 immune cells based on the ssGSEA scores.[25] The cancer immune cycle can be conceptualized as a sequential progression of events comprising the anticancer immune response. TIP systematically integrates two existing methodologies, namely, "ssGSEA" and "CIBERSORT", to monitor and analyze the proportion of tumor-infiltrating immune cells in the cancer immune cycle.[26]

2.8. Analysis of the receiver operating characteristic (ROC) curve

Data were evaluated using the pROC package, which included performing ROC analysis.[27] Then, the findings were plotted using ggplot2, a visualization tool, to evaluate the sensitivity and specificity of the six IIEGs. Outcomes were measured by calculating the area under the ROC curve (AUC), where variables displaying an AUC >0.6 demonstrated improved diagnostic capability in outcome prediction. A higher AUC, closer to 1, indicated a more positive diagnostic influence.

2.9. Data verification

In addition, we performed further verification in the clinical samples of HCC by quantitative real-time polymerase chain reaction (qRT-PCR), immunohistochemical staining, and Western blotting.

2.9.1. Patients and tissue specimens

All clinical samples were collected between May 2023 and June 2024 at The Third Affiliated Hospital of Sun Yat-sen University, Guangzhou, China. Ten pairs of HCC tissues and adjacent non-cancerous tissues were obtained to detect the expressions of six IIEGs using qRT-PCR. A total of 30 paraffin-embedded tissue samples were obtained from patients who were histopathologically diagnosed with primary HCC and had undergone curative surgery. Six paired HCC tissues and adjacent non-cancerous tissues were obtained immediately after surgery to detect the differential expression of glycosylphosphatidylinositol anchor attachment 1 (GPAA1) by Western blotting.

2.9.2. RNA isolation and qRT-PCR

Total RNA was isolated with TRIzol reagent (Thermo Fisher Scientific, Waltham, MA, USA), followed by cDNA synthesis using the HifairTM II 1st Strand cDNA Synthesis SuperMix Kit (Yeasen, Shanghai, China). qRT-PCR was performed using the ChamQ SYBR qPCR Master Mix (Vazyme, Nanjing, China) following the manufacturer's instruction. Normalization of mRNA expression was achieved using GAPDH as an internal reference. The primer sequences used are listed in Supplemental Table 2.

2.9.3. Immunohistochemistry (IHC) staining and scoring

The collected slides were subjected to a series of steps prior to IHC. First, the slides were baked at 60 °C for 3 h. Next, the slides were deparaffinised in xylene and rehydrated by progressive exposure to different concentrations of alcohol. The slides were then immersed in a 0.3% hydrogen peroxide solution at room temperature for 20 min to inhibit endogenous peroxidase activity. To retrieve the antigens, the slides were boiled for 30 min in a microwave using an ethylenediaminetetraacetic acid (EDTA) buffer with pH 8.0. After cooling to room temperature, the slides were incubated overnight at 4 °C in a humidity chamber (Shanghai Yiheng Scientific Instruments Co., Ltd., Shanghai, China) with a polyclonal antibody against centrosomal protein 55 (CEP55) (DF6224, ProteinTech Group, Chicago, IL, USA) and GPAA1 (10104-1-AP, ProteinTech Group, Chicago, IL, USA) for specific protein detection. The slides were then incubated with horseradish peroxidase from the DAKO ChemMate™ EnVision™ Detection Kit (Dako Denmark A/S) at 37 °C for 30 min. After three washes in PBST (phosphate-buffered saline with Tween 20) solution, the slides were stained with a 3,3′-diaminobenzidine (DAB) solution at room temperature for 2 min to visualise the detected proteins. Finally, Mayer's haematoxylin was used for nuclear counterstaining to enhance the visibility of tissue structures.

2.9.4. Western blotting

Tissue samples were dissolved in sodium dodecyl sulfate (SDS) lysis buffer, and the protein concentrations were determined with the BCA protein assay kit (Pierce, Rockford, IL, USA). Each protein sample (20 μg) was separated via electrophoresis in 10% SDS polyacrylamide gel for 2 h and subsequently transferred onto polyvinylidene fluoride (PVDF) membranes (Millipore, Bedford, MA, USA). The membranes were incubated overnight at 4 °C with a primary polyclonal antibody targeting GPAA1 (10104-1-AP, ProteinTech Group, Chicago, IL, USA) and GAPDH (Cell Signaling Technology, Danvers, MA, USA). The bands were visualized using an enhanced chemiluminescence system (Amersham Pharmacia Biotech, Sweden) after incubation with secondary antibody (Jackson ImmunoResearch, Philadelphia, PA, USA). Analysis of the gray values was performed utilizing Image J software (General Public License).

2.10. Statistical analysis

All calculations and statistical analyses were performed using R (version 4.3.1) (https://www.r-project.org/) and SPSS (version 25, IBM Corporation, Armonk, NY, USA). To assess the significance of continuous variables between the two groups, independent Student's *t*-tests were utilized for normally distributed variables, whereas the Mann–Whitney *U* test (i.e., Wilcoxon rank-sum test) was employed for nonnormally distributed variables. Paired-sample *t*-tests were used to assess the significance of variables in the validation experiment. The prognostic values of IIEG expression on overall survival (OS), disease-specific survival (DSS), and progression-free interval (PFI) were assessed using Cox regression analysis and Kaplan-Meier (K-M) curves. Time-dependent ROC curve analysis was performed to evaluate the 1-, 3-, and 5-year predictive ability of immune evasion-related genes for HCC outcomes. All statistical tests followed a two-tailed approach, and significance was considered at *P*-value <0.05.

3. Results

3.1. Expression and enrichment analysis of IIEGs

The study flowchart is shown in Fig. 1. By performing single-factoruniavariate regression analysis, a total of 63 IIEGs

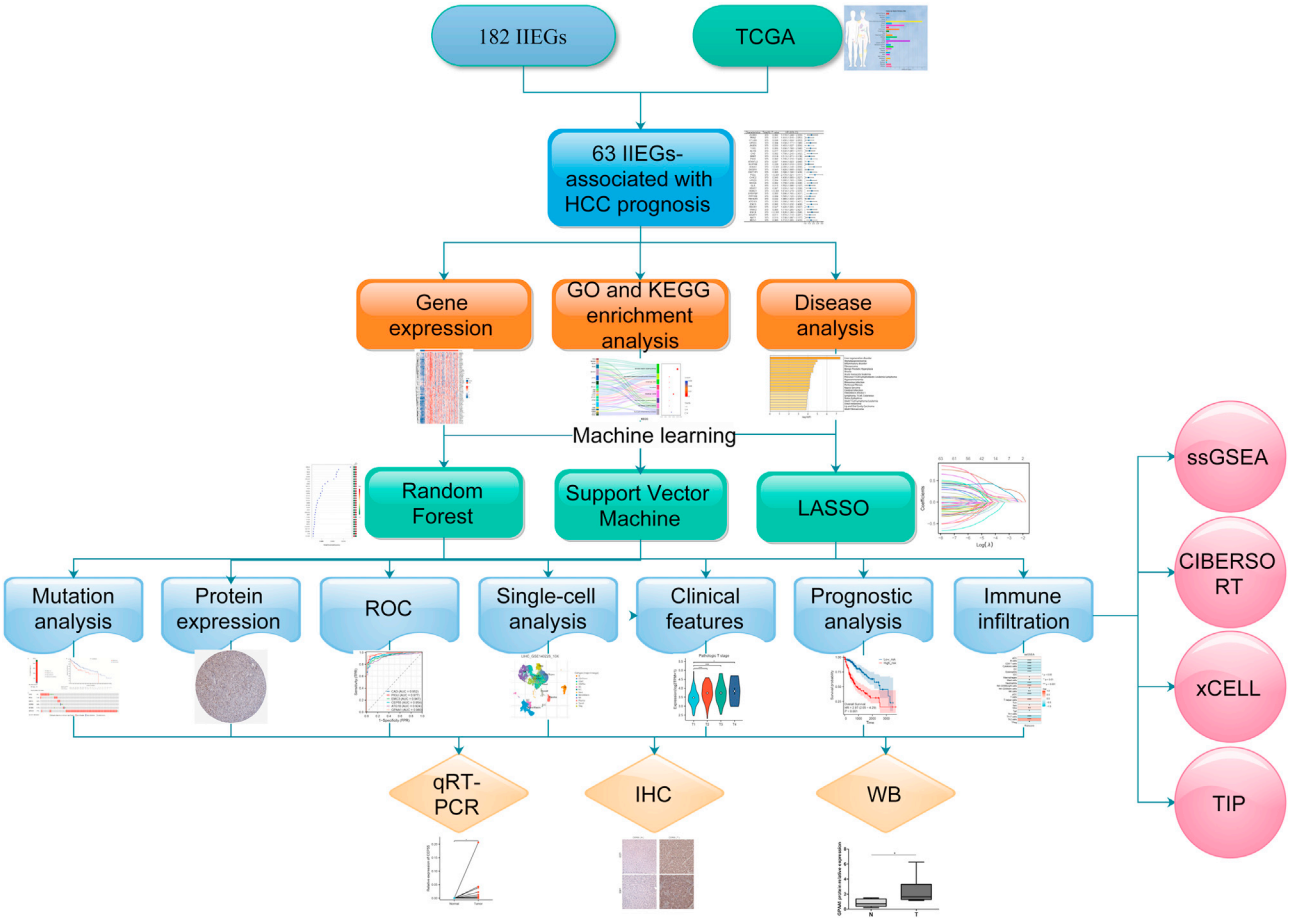

Fig. 1. Flow chart of the study. In this study, we selected 182 IIEGs from previous literature and utilized TCGA-liver hepatocellular carcinoma (LIHC) dataset to filter them to 63 IIEGs-associated with HCC prognosis by univariate analysis. Machine learning methods identified six key genes. We then performed mutation, protein expression, and ROC analyses, followed by single-cell profiling and clinical relevance studies. Finally, we confirmed IIEG expressions with qRT-PCR, immunohistochemistry (IHC), and Western blotting (WB), demonstrating their roles in HCC and immune evasion. Abbreviations: GO, Gene Ontology; HCC, hepatocellular carcinoma; IIEGs, intrinsic immune-evasion genes; KEGG, Kyoto Encyclopedia of Genes and Genomes; LASSO, least absolute shrinkage and selection operator; qRT-PCR, quantitative real-time polymerase chain reaction; ROC, receiver operating characteristic; ssGSEA, single-sample gene set enrichment analysis; TCGA, The Cancer Genome Atlas; TIP, tumor immunophenotype.

associated with HCC OS were identified from a pool of 182 IIEGs (Fig. 2A and B). The expression heatmap of these 63 IIEGs is presented in Fig. 2C. Subsequent GO (biological progress (BP), cellular component (CC), and molecular function (MF)) (Fig. 2D–F) and KEGG (Fig. 2G) enrichment analyses of these genes revealed that GO terms enriched in the study included protein lipidation, nuclear factor-kappa B (NF-kappa B) signaling, histone modification, T-cell receptor signaling, apoptotic signaling regulation, mitochondrion organization regulation, hepatocyte apoptosis, extrinsic apoptotic signaling regulation, and histone acetylation (Fig. 2D). Additionally, the KEGG pathways showed prominent enrichment in several signaling pathways, including the nucleotide-binding and oligomerization domain (NOD)-like receptor signaling pathway, glycosylphosphatidylinositol (GPI)-anchor biosynthesis, autophagy, ferroptosis, retinoic acid-inducible gene I (RIG-I)-like receptor signaling pathway, NF-kappa B signaling pathway, and neutrophil extracellular trap formation (Fig. 2G). Furthermore, the analysis using the DisGeNET database in the WebGestalt website indicated that these 63 IIEGs were significantly associated with liver regeneration disorder, inflammatory disorder, and various malignancies such as sarcoma, lymphoma, and melanoma (Fig. 2H).

3.2. Screening hub IIEGs by machine learning

Random forest, support vector machine, and least absolute shrinkage and selection operator (LASSO) regression analysis were employed to further identify hub genes from the initial 63 IIEGs. The random forest analysis identified 30 candidate genes (Fig. 3A). Similarly, the support vector machine analysis identified 30 candidate genes (Fig. 3B). The LASSO regression analysis identified eight candidate genes (Fig. 3C and D). By intersecting the genes selected by these three machine-learning methods, six hub genes, including carbamoyl-phosphate synthetase 2, aspartate transcarbamylase, and dihydroorotase (CAD), phosphatidylinositol glycan anchor biosynthesis class U (PIGU), endoplasmic reticulum membrane protein complex subunit 3 (EMC3), CEP55, autophagy-related 10 (ATG10), and GPAA1, were identified (Fig. 2E). The chromosomal distribution of these genes is illustrated in Fig. 3F. To assess the diagnostic accuracy for HCC, the ROC curve was plotted

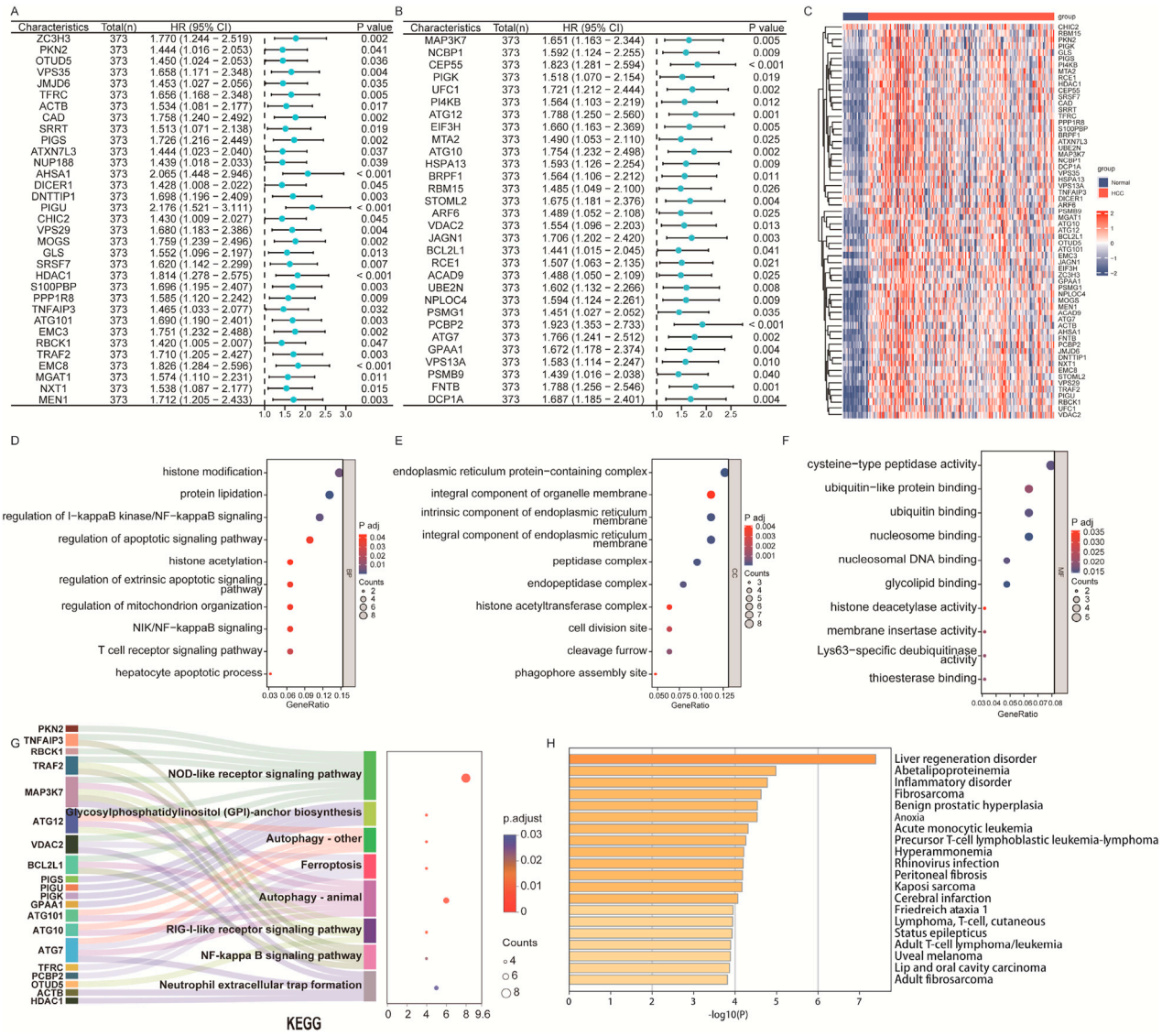

Fig. 2. Expression and enrichment analysis of intrinsic immune-evasion genes (IIEGs). (A, B) Identification of OS-associated IIEGs via the univariate Cox regression analysis. **(C)** The heatmap displayed the expression of a total of 63 IIEGs in HCC and normal samples. **(D–G)** GO (D–F) and KEGG (G) enrichment analyses of 63 IIEGs. **(H)** Disease enrichment analysis of 63 IIEGs in DisGeNET. Abbreviations: ATG, autophagy-related; CAD, carbamoyl-phosphate synthetase 2, aspartate transcarbamylase, and dihydroorotase; CEP55, centrosomal protein 55; CI, confidence interval; EMC3, endoplasmic reticulum membrane protein complex subunit 3; GO, Gene Ontology; GPAA1, glycosylphosphatidylinositol anchor attachment 1; HCC, hepatocellular carcinoma; HR, hazard ratio; KEGG, Kyoto Encyclopedia of Genes and Genomes; NF-kappa B, nuclear factor-kappa B; NOD, nucleotide-binding and oligomerization domain; OS, overall survival; PIG, phosphatidylinositol glycan; RIG-I, retinoic acid-inducible gene I.

for these six genes (Fig. 3G). Notably, all six IIEGs exhibited an AUC >0.92, indicating a high diagnostic accuracy for HCC. Based on these results, a risk model was constructed using the six hub genes. The risk score for each patient can be calculated using the following formula: risk score = (0.101374716 × CAD) + (0.339327368 × PIGU) + (0.085473101 × EMC3) + (0.122379030 × CEP55) + (0.322182048 × ATG10) + (0.032768301 × GPAA1).

3.3. Protein expression levels of IIEGs in HCC

After determining the transcriptional expression of the six IIEGs in HCC, the protein expression patterns of these genes were analyzed using the HPA and UALCAN databases (Fig. 4A and B). Within the HPA database, the protein levels of CAD, PIGU, EMC3, CEP55, and GPAA1 were upregulated in HCC tissues comparison with these in normal tissues, except for ATG10 (Fig. 4A). In addition, the UALCAN database displayed high protein levels of CAD, PIGU, EMC3, and GPAA1 in primary tumors compared with these in normal tissues, with CEP55 showing no expression difference (ATG10 showing a deficiency) (Fig. 4B).

3.4. Single-cell analysis of IIEGs in HCC

The GSE140228 dataset from TISCH2 database was comprehensively analyzed to gain further insights into the expression profiles of these six IIEGs at the single-cell level in HCC. This dataset was carefully examined to identify 21 distinct cell clusters, predominantly composed of immune cells (Fig. 5A). Subsequent annotation revealed 12 distinct cell types among these cell clusters (Fig. 5B). GPAA1 and EMC3 were highly expressed in nearly all immune cell types (Fig. 5C and D), and PIGU, CAD, and ATG10 were upregulated in several immune cell types (Fig. 5E–G). In addition, CEP55 was predominantly expressed in the Tprolif cell cluster (Fig. 5H). The gene signature labeling based on the average

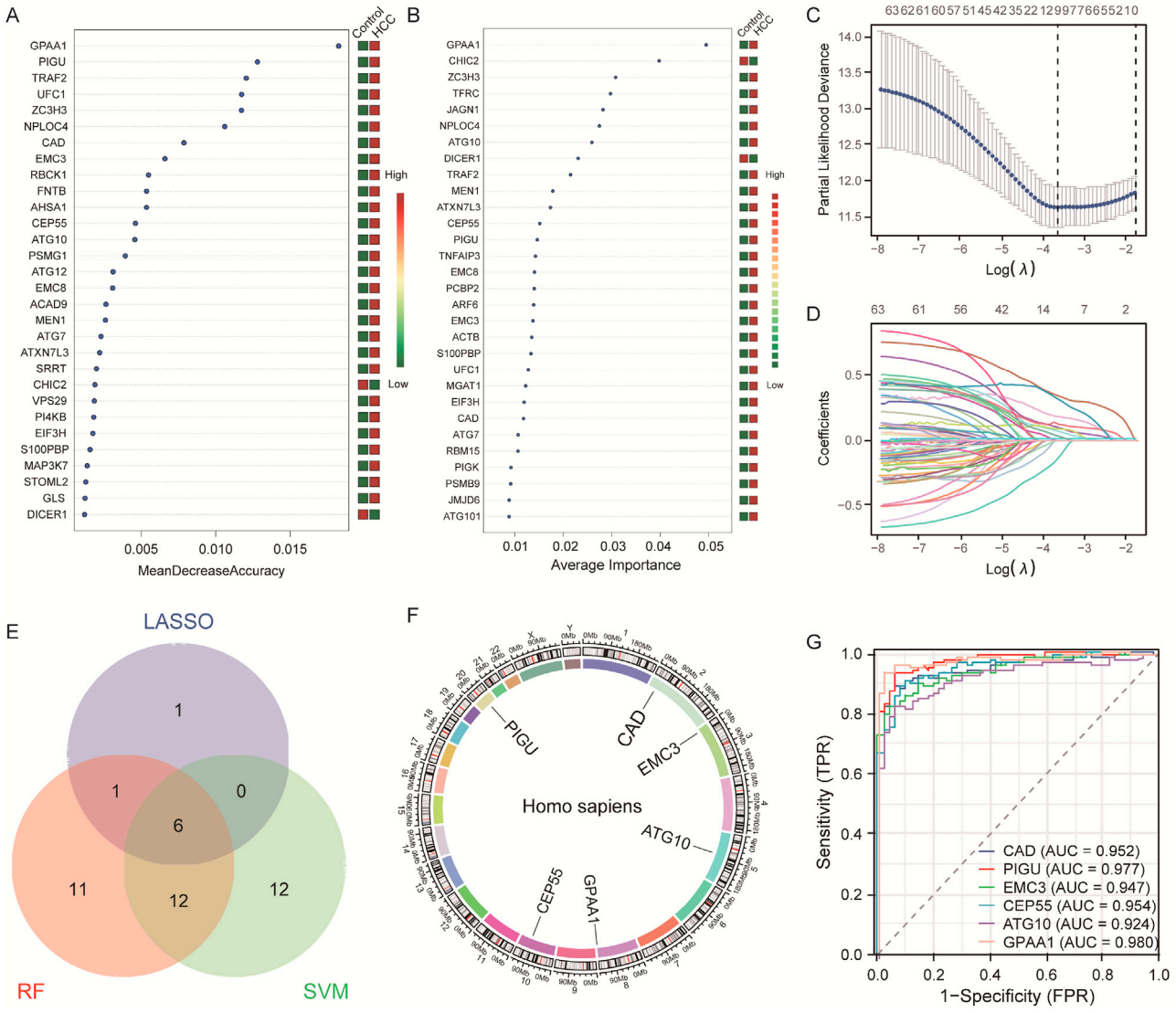

Fig. 3. Screening hub IIEGs by machine learning. (A) Top 30 candidate genes screened by random forest (RF). **(B)** Top 30 candidate genes screened by support vector machine (SVM). **(C, D)** LASSO Cox regression analysis of 63 IIEGs. **(E)** The Venn diagram illustrates the overlap of the gene sets analyzed by LASSO regression, RF, and SVM. **(F)** Chromosome distribution of six IIEGs in patients with HCC. **(G)** Diagnostic ROC curve of the six IIEGs. Abbreviations: ATG10, autophagy-related 10; CAD, carbamoyl-phosphate synthetase 2, aspartate transcarbamylase, and dihydroorotase; CEP55, centrosomal protein 55; EMC3, endoplasmic reticulum membrane protein complex subunit 3; FPR, false positive rate; GPAA1, glycosylphosphatidylinositol anchor attachment 1; HCC, hepatocellular carcinoma; IIEGs, intrinsic immune-evasion genes; LASSO, least absolute shrinkage and selection operator; PIGU, phosphatidylinositol glycan anchor biosynthesis class U; ROC, receiver operating characteristic; TPR, true positive rate.

expression levels of these six genes, is illustrated in Fig. 5I. The high expression of IIEGs in nearly all immune cell types proposed their crucial role in regulating the immune suppression process within the TME. This may include the inhibition of immune cell activation, promoting the proliferation and function of immune inhibitory cells, and modulation of signaling pathways associated with immune evasion.

To further explore the significance of the Tprolif cells, which exhibited the highest expression in the gene signature label, cell communication analysis was performed. This analysis revealed strong correlations between Tprolif cells and different cell types including $CD4^+$ T cells, $CD8^+$ T cells, monocytes/macrophages, and natural killer (NK) cells (Fig. 5J). Upregulated KEGG gene-set analysis found associations between Tprolif cells and DNA replication, cell cycle, oxidative phosphorylation, and homologous recombination (Fig. 5K). Upregulated HALLMARK gene-set analysis revealed associations between Tprolif cells and apical junction, glycolysis, oxidative phosphorylation, E2F targets, G2M checkpoint, MYC targets, mitotic spindle, and mechanistic target of rapamycin complex 1 (mTORC1) signaling (Fig. 5L).

3.5. Mutation analysis of IIEGs

The mutation status of IIEGs was obtained from cBioPortal. Among the patients, 23.4% exhibited genetic alterations, with amplification as the most common mutation among IIEG isoforms (Fig. 6A). Then, we categorized the samples into altered and unaltered groups based on the presence and absence of genetic alterations in these six IIEGs. The results showed that the altered group ($n = 86$) had a worse prognosis compared with the unaltered group ($n = 279$) ($P = 0.003203$, Fig. 6B). Furthermore, *GPAA1* mutations were the most prevalent, accounting for 17% of all mutations. These mutations can involve both amplifications and missense mutations. PIGU and EMC3 only exhibited amplification mutations, with

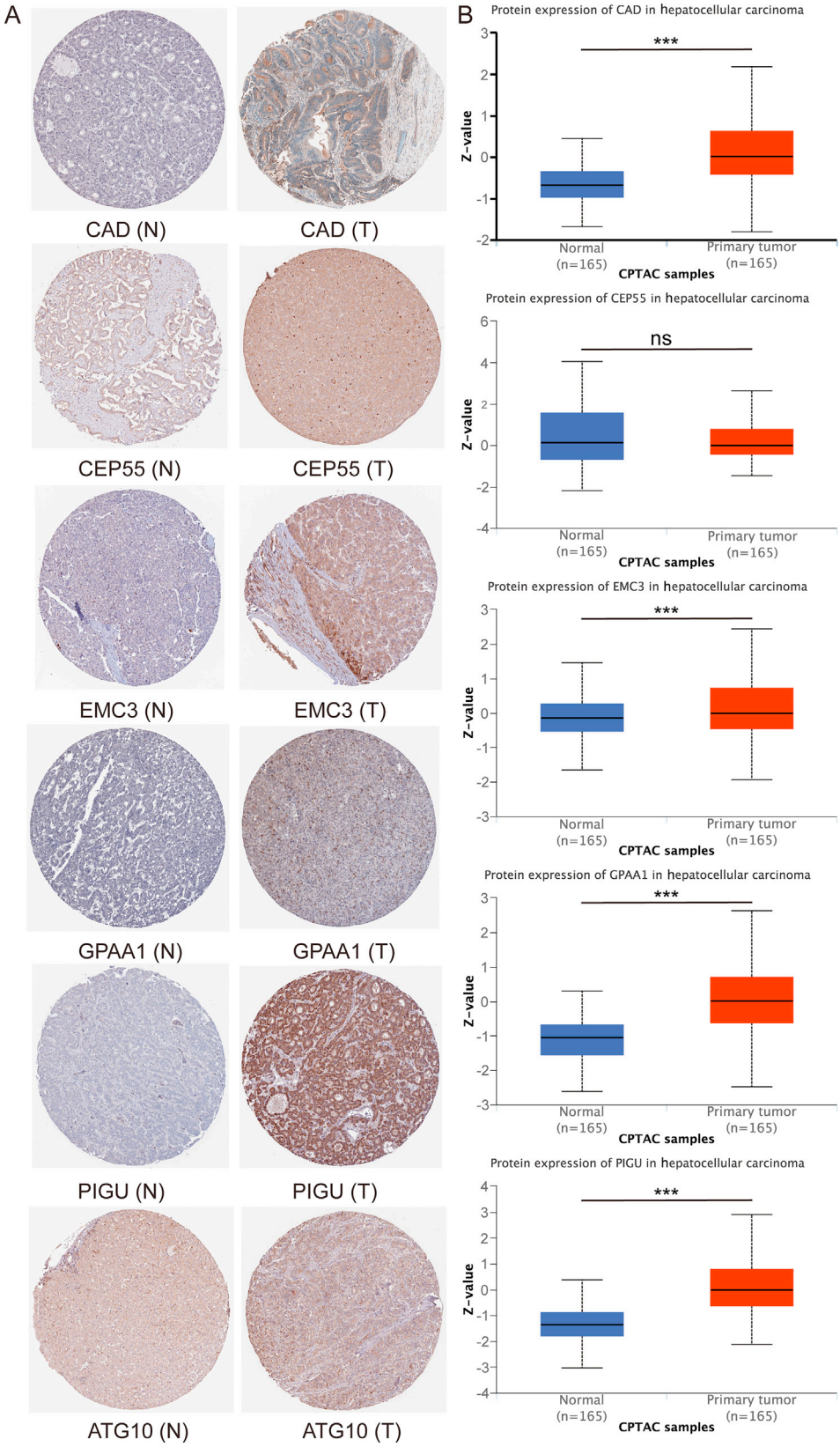

Fig. 4. Protein expression levels of six IIEGs in HCC. (A) The protein expressions of CAD, CEP55, EMC3, GPAA1, and PIGU were upregulated in the HCC tissues (T) compared with these in the normal tissues (N) from the Human Protein Atlas (HPA) database (200× magnification). **(B)** The protein levels of CAD, EMC3, GPAA1, and PIGU were significantly upregulated in the primary tumors compared with these in the normal tissues from the UALCAN database. $^{***}P < 0.001$. ns, not significant. Abbreviations: ATG10, autophagy-related 10; CAD, carbamoyl-phosphate synthetase 2, aspartate transcarbamylase, and dihydroorotase; CEP55, centrosomal protein 55; EMC3, endoplasmic reticulum membrane protein complex subunit 3; GPAA1, glycosylphosphatidylinositol anchor attachment 1; HCC, hepatocellular carcinoma; IIEGs, intrinsic immune-evasion genes; PIGU, phosphatidylinositol glycan anchor biosynthesis class U.

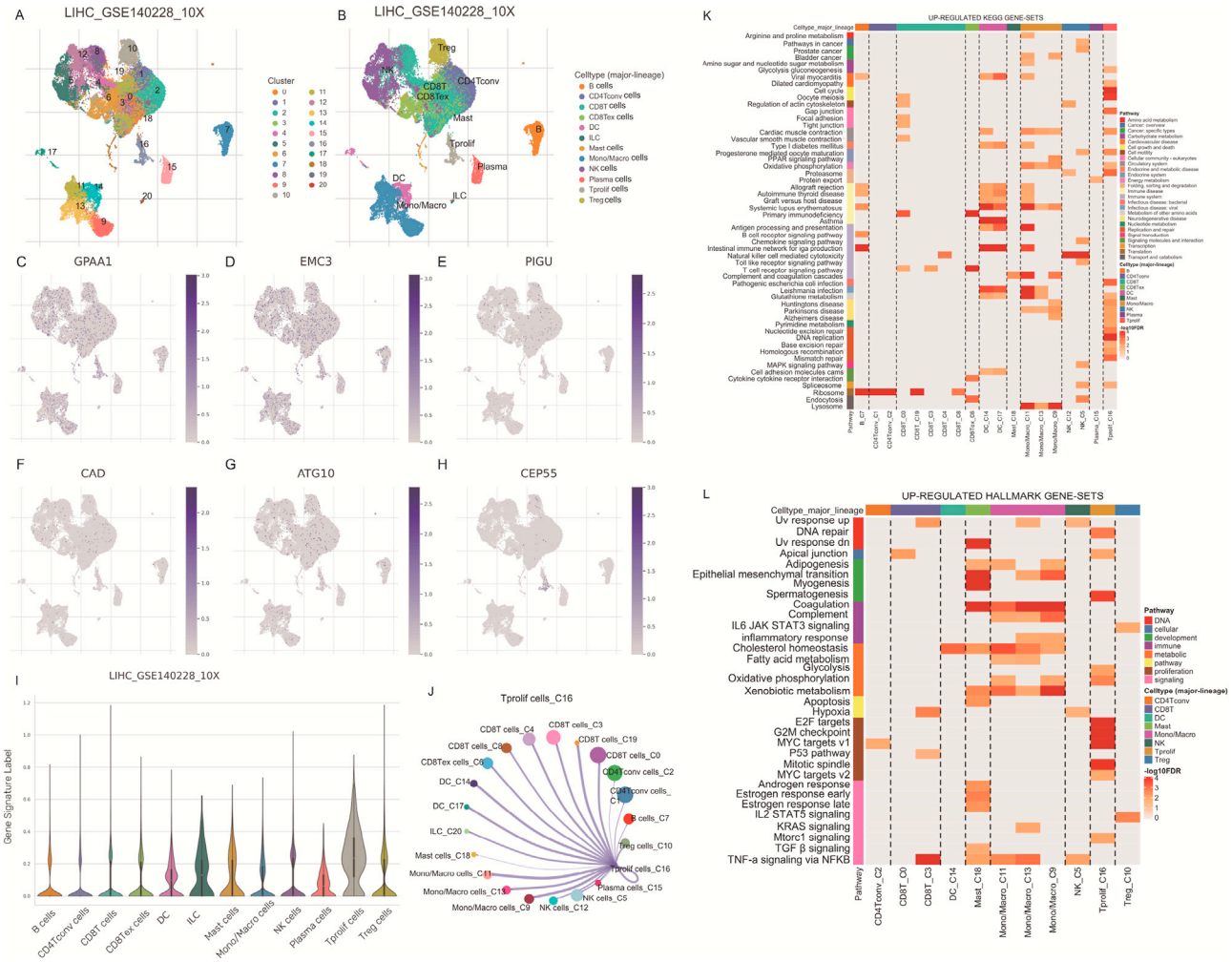

Fig. 5. Cellular-level expression of IIEGs in hepatocellular carcinoma (HCC). (A) The UMAP plot of 21 distinct cell clusters based on HCC dataset GSE140228. **(B)** The UMAP plot presented by 12 cell types. **(C–H)** Expression of six IIEGs in 12 subpopulations of cells from the HCC dataset GSE140228. **(I)** Average gene expression of the six IIEGs in 12 subpopulations of cells. **(J)** Intercellular communication between Tprolif cells and different cell types based on HCC dataset GSE140228. **(K)** Upregulated KEGG gene-set analysis. **(L)** Upregulated HALLMARK gene-set analysis. Abbreviations: ATG10, autophagy-related 10; CAD, carbamoyl-phosphate synthetase 2, aspartate transcarbamylase, and dihydroorotase; CEP55, centrosomal protein 55; DC, dendritic cells; EMC3, endoplasmic reticulum membrane protein complex subunit 3; GPAA1, glycosylphosphatidylinositol anchor attachment 1; IIEGs, intrinsic immune-evasion genes; LIHC, liver hepatocellular carcinoma; NK, natural killer; PIGU, phosphatidylinositol glycan anchor biosynthesis class U; Tconvs, conventional T cells; Tex, exhausted T; Treg, regulatory T.

mutation rates of 1.4% and 0.8%, respectively. CEP55 had a mutation rate of 0.8%, which included deep deletions and missense mutations. CAD exhibited a mutation rate of 4%, which covered amplifications and missense mutations. Finally, ATG10 had a mutation rate of 1.1%, which encompassed amplifications, missense mutations, and deep deletions (Fig. 6C). In addition, differential analysis was conducted between the selected groups of genomic alterations and displayed clinical information. Associations were found between the combination of mutations in these six IIEGs and surgical margin resection status ($P = 0.0181$, Fig. 6D), optimum cutting temperature (Oct) embedded ($P = 0.0375$, Fig. 6E), fraction genome altered ($P = 0.0263$, Fig. 6F), and laboratory procedure albumin result upper limit of the normal value ($P = 0.0489$, Fig. 6G).

3.6. *Independent prognostic analysis and clinical characteristics of the risk score model*

The expression of the IIEG signature in different clinical features was analyzed. The expression level of the gene signature with higher T stage, with the highest expression observed in T4 stage, gradually increased (Fig. 7A). As regards immune subtype, the IIEG signature demonstrated higher expression levels in C1, C2, and C4, whereas the expression was the lowest in C3 and C6 (Fig. 7B). Within the molecular subtype, the IIEG signature exhibited the highest expression in iCluster3 (Fig. 7C). These observations indicate a significant correlation between the IIEG signature and T stage, immune subtype, and molecular subtype. Moving forward, the prognostic significance of the IIEG risk model was evaluated in the TCGA cohort. In this cohort, patients were divided into the low- and high-risk groups based on their risk scores, which were determined using the expression levels of the IIEG signature. K-M curves showed a significant association between the high-risk group and worse OS, DSS, and PFI (Fig. 7D–F). Additional graphical representations (Fig. 7G–I) provided further evidence of more deaths and higher expression levels of the six IIEGs in the high-risk group.

ROC curves were also generated to assess the prognostic significance of our risk model. For OS, the AUC values for the risk score at 1, 3, and 5 years were 0.779, 0.714, and 0.707, respectively (Fig. 7J). Similarly, for DSS, the AUC values for the risk score at 1, 3, and 5 years were 0.805, 0.734, and 0.693, respectively (Fig. 7K). Regarding PFI, the AUC scores for the risk score at 1, 3, and 5 years

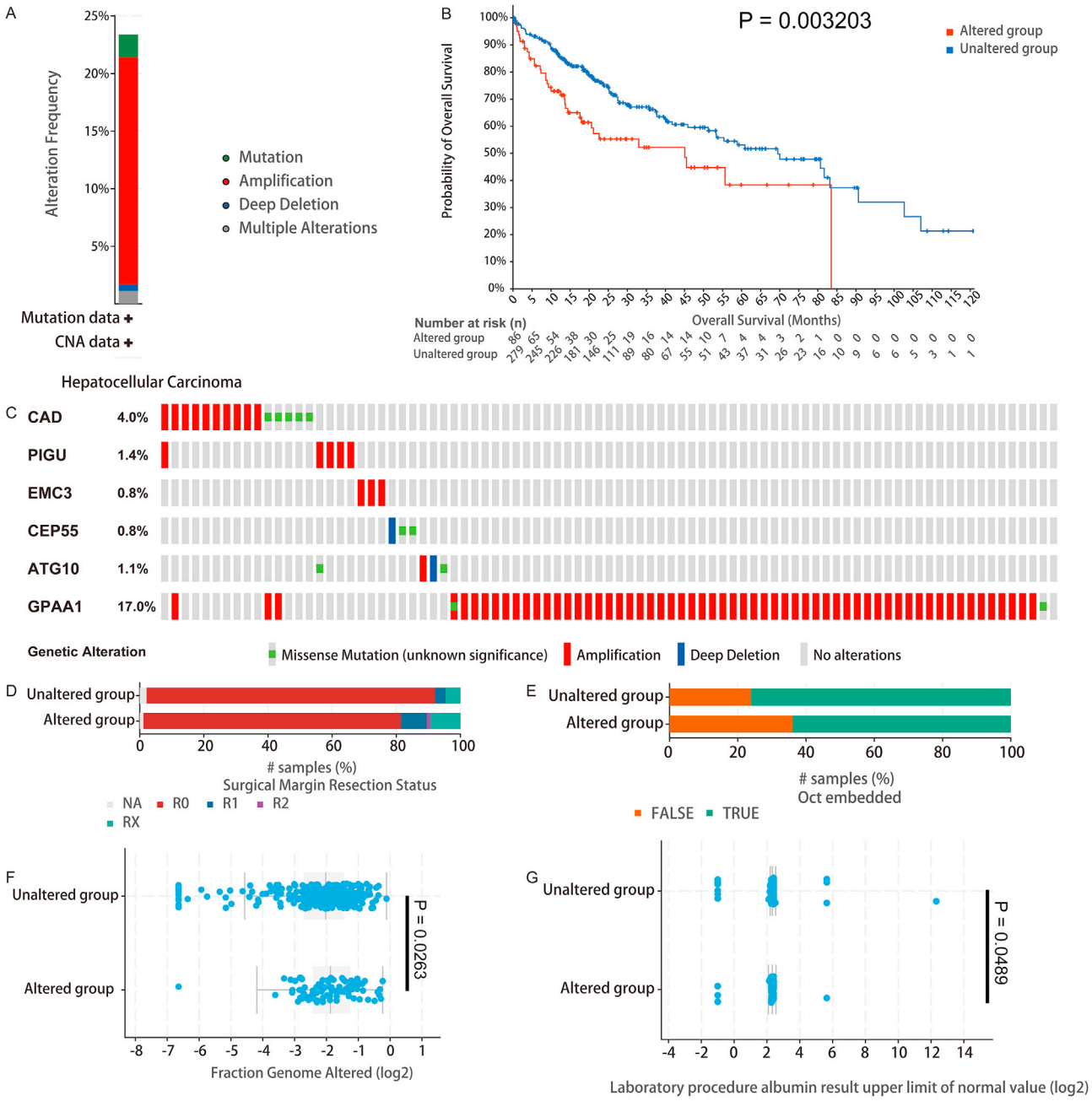

Fig. 6. Mutation analysis of IIEGs in HCC. (A) Mutation frequency of the six IIEGs. **(B)** Overall survival rates of HCC patients with or without genetic alterations in the six IIEGs. **(C)** Mutation details of every IIEG in each individual sample. **(D)** Association between the IIEG signature and surgical margin resection status ($P = 0.0181$). **(E)** Association between the IIEG signature and Oct embedded ($P = 0.0375$). **(F)** Association between the IIEG signature and fraction genome altered. **(G)** Association between the IIEG signature and laboratory procedure albumin result upper limit of the normal value. Abbreviations: ATG10, autophagy-related 10; CAD, carbamoyl-phosphate synthetase 2, aspartate transcarbamylase, and dihydroorotase; CEP55, centrosomal protein 55; CNA, copy number alteration; EMC3, endoplasmic reticulum membrane protein complex subunit 3; GPAA1, glycosylphosphatidylinositol anchor attachment 1; HCC, hepatocellular carcinoma; IIEGs, intrinsic immune-evasion genes; Oct, optimum cutting temperature; PIGU, phosphatidylinositol glycan anchor biosynthesis class U.

were 0.682, 0.640, and 0.714, respectively (Fig. 7L). Taken together, these results confirm the predictive accuracy and robustness of our proposed risk score model.

3.7. Relationship between the IIEG risk score model and tumor immune microenvironment and immune checkpoint genes

The immune cells present in the TME significantly influence the tumor behavior.[28–30] In this study, several algorithms (ssGSEA, CIBERSORT, xCELL, and TIP) were utilized to explore the relationship between the prognostic risk assessment model and immune cell infiltration. We aimed to determine whether the IIEG risk score model provides insights into the status of the tumor immune microenvironment. In the ssGSEA and CIBERSORT analyses, a positive correlation was observed between the prognostic risk score model and macrophages as well as T follicular helper (TFH) cells and a negative correlation with NK cells (Fig. 8A and B). Notably, CIBERSORT and xCELL analyses showed a positive correlation between the prognosis risk score model and activated memory $CD4^+$ T cells (Fig. 8B and C). In the CIBERSORT analysis, a

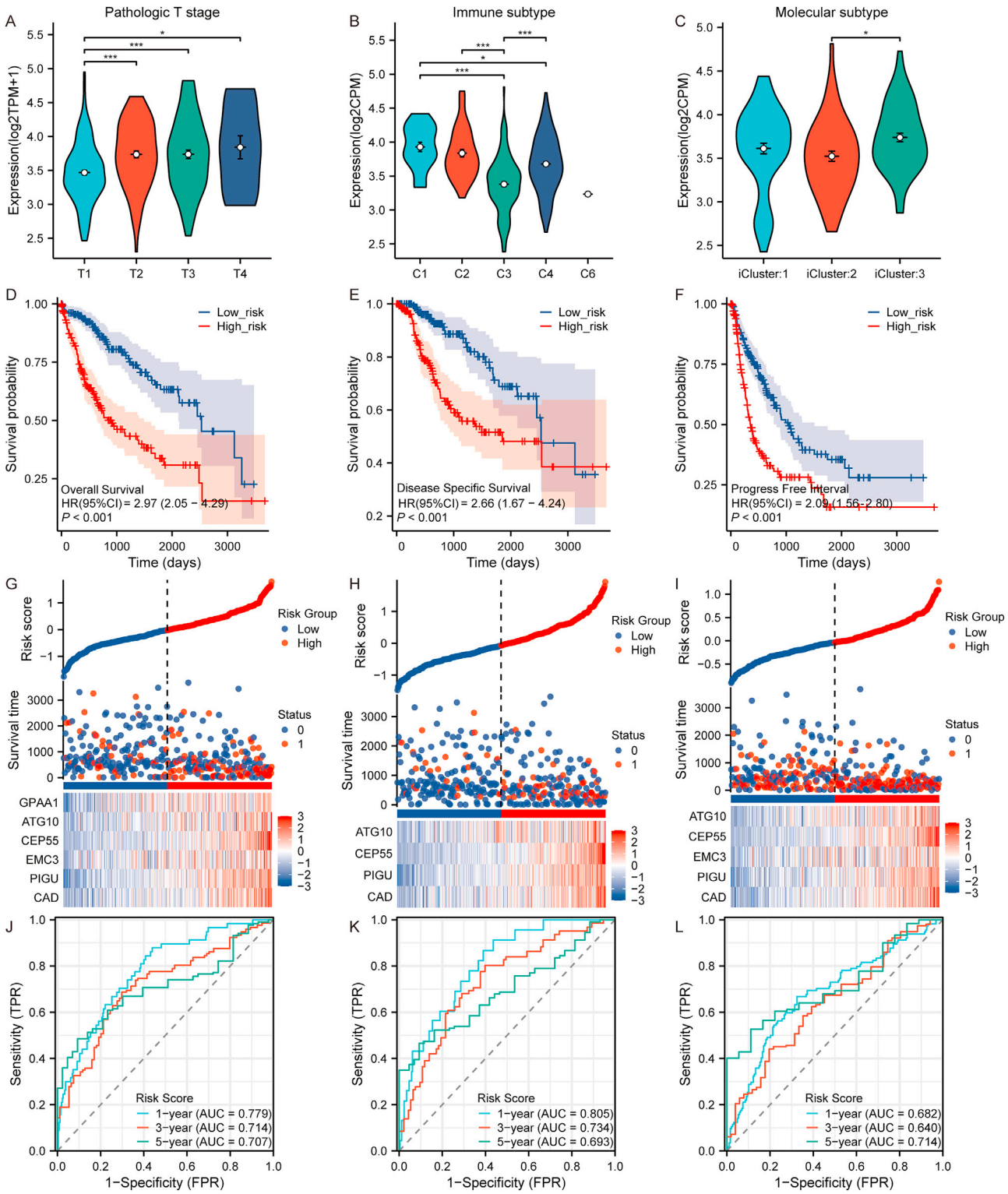

Fig. 7. Clinical relevance and prognostic value of IIEG signature. (A) Correlation between the IIEG signature and tumor stage in HCC. **(B)** Analysis of the IIEG signature in immune subtype. **(C)** Analysis of the IIEG signature in molecular subtype. **(D–F)** Kaplan–Meier plots depicting the OS (D), DSS (E), and PFI (F) of individuals categorized into the high- and low-risk cohorts. **(G–I)** Distribution of the risk score and correlation between survival time (G: OS, H: DSS, I: PFI) and status, and heatmaps of IIEG signature expressions in patients with HCC. **(J–L)** Time-dependent survival ROC curves predicting 1-, 3-, and 5-year OS (J), DSS (K), and PFI (L) in patients with HCC based on IIEG signature expression levels. $^{*}P < 0.05$, $^{***}P < 0.001$. Abbreviations: ATG10, autophagy-related 10; AUC, area under the receiver operating characteristic curve; CAD, carbamoyl-phosphate synthetase 2, aspartate transcarbamylase, and dihydroorotase; CEP55, centrosomal protein 55; CI, confidence interval; DSS, disease-specific survival; EMC3, endoplasmic reticulum membrane protein complex subunit 3; FPR, false positive rate; GPAA1, glycosylphosphatidylinositol anchor attachment 1; HCC, hepatocellular carcinoma; HR, hazard ratio; IIEG, intrinsic immune-evasion gene; OS, overall survival; PFI, progression-free interval; PIGU, phosphatidylinositol glycan anchor biosynthesis class U; ROC, receiver operating characteristic; TPR, true positive rate.

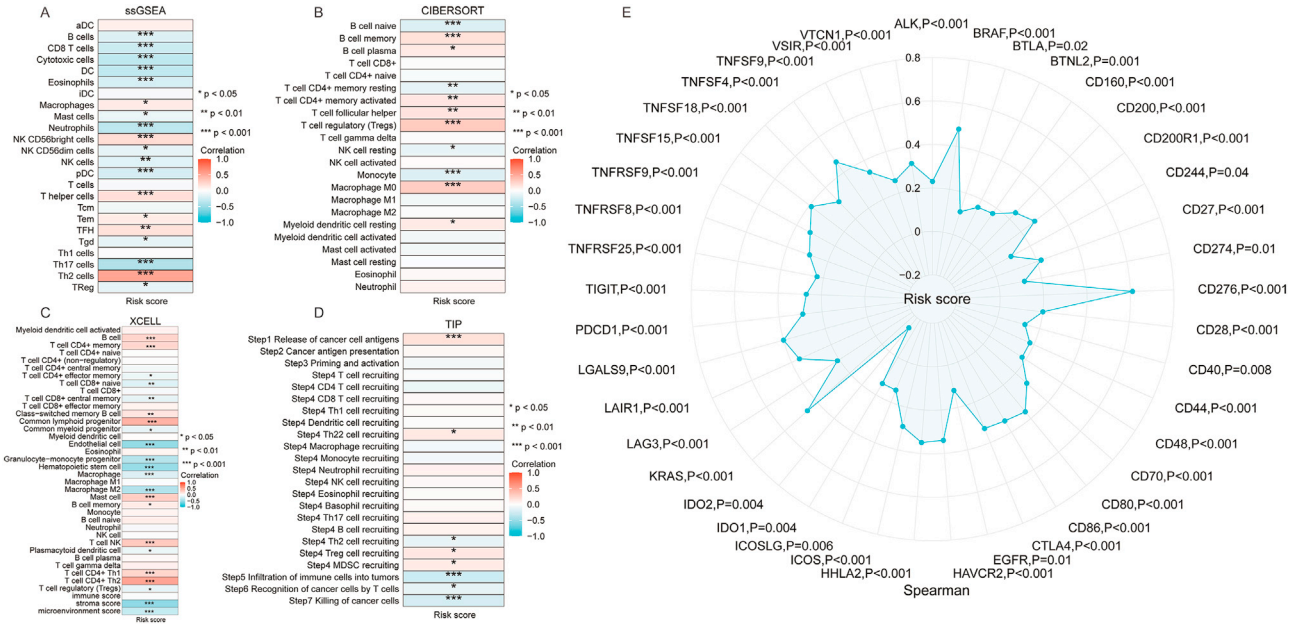

Fig. 8. Characteristics of IIEG risk score associated with tumor immune microenvironment and immune checkpoint genes. (A) Analysis of the relationship between the IIEG risk score and immune cells by the ssGSEA algorithm. **(B)** Analysis of the relationship between the IIEG risk score and immune cells by the CIBERSORT algorithm. **(C)** Analysis of the relationship between the IIEG risk score and immune cells by the xCELL algorithm. **(D)** Analysis of the relationship between the IIEG risk score and anticancer immune response by the TIP algorithm. **(E)** Analysis of the relationship between the IIEG risk score and immune checkpoint genes. $^{*}P < 0.05$, $^{**}P < 0.01$, $^{***}P < 0.001$. Abbreviations: DC, dendritic cells; IIEG, intrinsic immune-evasion gene; MDSC, myeloid-derived suppressor cell; NK, natural killer; ssGSEA, single-sample gene set enrichment analysis; TFH, T follicular helper; TIP, tumor immunophenotype.

negative correlation with naive B-cell and a positive correlation with memory B-cell and plasma cell were found (Fig. 8B).

Using the TIP algorithm, a positive correlation was discovered among the prognostic risk score model and release of cancer cell antigen, Th22 cell recruitment, Treg cell recruitment, and myeloid-derived suppressor cell (MDSC) recruitment (Fig. 8D). Conversely, a negative correlation was observed with infiltration of immune cells into tumors, recognition of cancer cells by T cells, and killing cancer cell (Fig. 8D). This further supports the notion that immune escape-related genes may impede the immune system, promoting tumor immune evasion and tumor development. To deepen our understanding, the correlation between this prognostic model and immune checkpoint genes was evaluated. Interestingly, a positive correlation was found between the prognostic model and 40 immune checkpoint genes, with emphasis on well-known immune checkpoint genes such as *PDCD1*, *HAVCR2*, *TIGIT*, *LAG3*, and *CTLA4*. These correlations were significant, with all correlation *P*-values <0.001 (Fig. 8E).

3.8. Validation of IIEG expression in HCC

After analyzing the patterns of immune cell infiltration and their correlation with the prognostic model, we validated the expression levels of the six IIEGs using qRT-PCR (Fig. 9A–F). In this study, qRT-PCR experiments were performed on samples obtained from 10 pairs of HCC tissues and adjacent non-cancerous tissues to gain further insight into the role of these genes in HCC progression and immune evasion. GPAA1 and CEP55 were significantly overexpressed in HCC compared with these in adjacent non-cancerous tissues ($P < 0.05$) (Fig. 9A and B). Conversely, the expression levels of the other four genes (CAD, EMC3, ATG10, and PIGU) examined did not exhibit significant variations between tumor and adjacent non-cancerous tissues (Fig. 9C–F), possibly due to the limited sample size. Furthermore, protein expression analysis of GPAA1 and CEP55 via immunohistochemistry revealed a significant increase in CEP55 protein levels in liver tissues of patients with HCC compared with normal tissues (Fig. 9G). GPAA1 protein expression was weakly positive in normal tissues but showed strong positive expression in HCC tissues (Fig. 9H). Western blotting analysis was performed on six paired HCC and adjacent non-cancerous tissues (Supplemental Fig. 1). The bar graphs showed an upregulation of GPAA1 expression in HCC tissues compared with their adjacent non-cancerous tissues ($P < 0.05$) (Fig. 9I).

4. Discussion

This study focused on the expression and enrichment analysis of IIEGs in HCC to elucidate their role in tumor progression and immune evasion. Through comprehensive analysis, 63 IIEGs associated with HCC OS were identified, and their functional roles were characterized through GO and KEGG enrichment analyses. These IIEGs were enriched in various biological processes and signaling pathways involved in cancer progression, such as the NF-kappa B signaling pathway. Given the inflammatory microenvironment and various oncogenic mutations, many human cancers exhibit constitutive NF-kappa B activity. The activity of NF-kappa B promotes tumor cell proliferation, inhibits apoptosis, induces angiogenesis, induces epithelial–mesenchymal transition (EMT), and facilitates distant metastasis.[31–33]

In addition, three machine learning methods were utilized to identify core genes within the cohort of 63 IIEGs, identifying six pivotal genes: *CAD*, *PIGU*, *EMC3*, *CEP55*, *ATG10*, and *GPAA1*. These genes showed remarkable diagnostic efficacy for HCC and were incorporated into a risk model for prognostic evaluation. Further investigations of protein expression levels and single-cell expression profiles of these genes provided additional understanding of their roles in HCC pathogenesis and immune system evasion. Furthermore, our mutational analysis revealed genetic modifications in a subset of patients, which highlight the potential prognostic relevance of these alterations in HCC. The stratification of

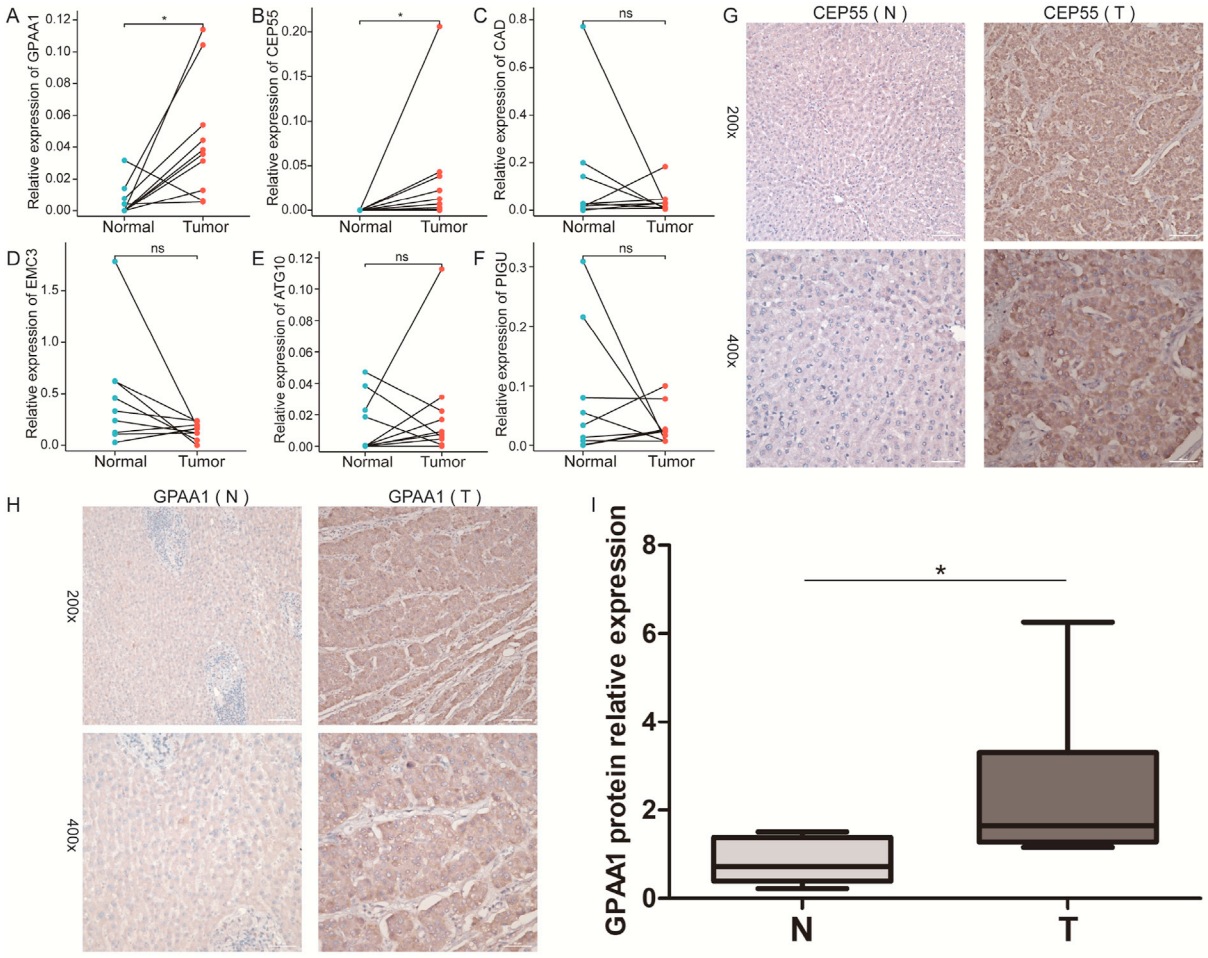

Fig. 9. mRNA and protein expressions of IIEGs in HCC and adjacent non-cancerous tissues. (A–F) The mRNA expressions of GPAA1 (A), CEP55 (B), CAD (C), EMC3(D), ATG10 (E), and PIGU (F) were detected by quantitative real-time polymerase chain reaction. **(G)** Protein expression of CEP55 was detected by immunohistochemistry staining in HCC (T) and adjacent non-cancerous tissues (N), and brown color indicates a positive staining. **(H)** Protein expression of GPAA1 was tested by immunohistochemistry in HCC (T) and adjacent non-cancerous tissues (N), and brown color indicates a positive staining. **(I)** The quantitative protein expression of GPAA1 is shown in HCC (T) and adjacent non-cancerous tissues (N). $^{*}P < 0.05$. ns, not significant. Abbreviations: ATG10, autophagy-related 10; CAD, carbamoyl-phosphate synthetase 2, aspartate transcarbamylase, and dihydroorotase; CEP55, centrosomal protein 55; EMC3, endoplasmic reticulum membrane protein complex subunit 3; GPAA1, glycosylphosphatidylinositol anchor attachment 1; HCC, hepatocellular carcinoma; IIEGs, intrinsic immune-evasion genes; PIGU, phosphatidylinositol glycan anchor biosynthesis class U.

patients according to the presence or absence of genetic alterations in the six core genes further underscored their correlation with clinical outcomes and tumor characteristics.

Moreover, this study investigated the association between the prognostic IIEG signature and the tumor immune microenvironment and immune checkpoint genes. Using different algorithms, a positive correlation was observed between the IIEG signature and Th2 cells and a negative correlation with cytotoxic cells including $CD8^{+}$ T and NK cells. Th2 cells are integral to the inflammatory mechanisms of cancer, particularly through their ability to drive tumor growth by converting M1 into M2 macrophages with immunosuppressive properties.[34] The production of interleukin-4 by Th2 cells has been associated with increased tumor invasiveness, highlighting the importance of IIEGs in shaping the immune response within the TME. This study also identified a strong association between the IIEG signature and several immune checkpoint genes, indicating their promise as viable targets for therapeutic intervention in HCC.

Furthermore, constraints inherent in this study must be recognized. The primary limitation is the reliance on bioinformatics analysis and publicly available datasets, which, although robust, are exposed to the inherent biases and variations in the source material. Consequently, our findings are correlative and require further validations through experimental methodologies, including *in vitro* and *in vivo* studies, to confirm the biological significance and functional roles of the identified IIEGs.

5. Conclusions

In summary, the six critical IIEGs, including GPAA1, CEP55, CAD, PIGU, EMC3, and ATG10, linked to the prognosis of HCC and evasion of immune responses were identified. The utilization of the IIEG risk score model as a novel prognostic index, together with its significance as a valuable biomarker for immunotherapy in HCC, provides benefit for patients with HCC in determining therapeutic strategies for clinical application. These findings elucidate the intricate interactions between tumor cells and the immune microenvironment in HCC prognosis and provide a basis for the development of innovative prognostic markers and therapeutic approaches targeting immune evasion mechanisms.

Data availability statement

Data are contained in the article or supplementary material. The data generated and analyzed in this study are available on request from the corresponding authors. Some data were obtained from online databases, including TCGA, HPA, cBioPortal, UALCAN, TISCH2, and WebGestalt.

Authors' contributions

Jiani Wang, Xiaopeng Chen, and Donghao Wu contributed equally to this work. **Jiani Wang:** Data collection, Bioinformatics analysis, Interpretation, Writing-original draft. **Xiaopeng Chen:** Data curation, Validation. **Donghao Wu:** Data curation, Validation. **Changchang Jia:** Conceptualization, Formal analysis, Funding acquisition. **Qinghai Lian:** Conceptualization, Formal analysis. **Yuhang Pan:** Resources, Supervision, Validation. **Jiumei Yang:** Conceptualization, Data analysis, Supervision, Project administration, Writing-review & editing.

Declaration of competing interest

The authors declare that they have no conflict of interest.

Acknowledgements

This work was granted by the Natural Science Foundation of Guangdong Province (No. 2017A030310252, No. 2022A1515012650) and the Science and Technology Program of Guangzhou (No. 2024A03J0919).

Appendix A. Supplementary data

Supplementary data to this article can be found online at https://doi.org/10.1016/j.livres.2024.11.001.

References

1. Nguyen PHD, Wasser M, Tan CT, et al. Trajectory of immune evasion and cancer progression in hepatocellular carcinoma. *Nat Commun*. 2022;13:1441. https://doi.org/10.1038/s41467-022-29122-w.
2. Yang JD, Hainaut P, Gores GJ, Amadou A, Plymoth A, Roberts LR. A global view of hepatocellular carcinoma: trends, risk, prevention and management. *Nat Rev Gastroenterol Hepatol*. 2019;16:589–604. https://doi.org/10.1038/s41575-019-0186-y.
3. Yang F, Lian Q, Ni B, et al. MUTYH is a potential prognostic biomarker and correlates with immune infiltrates in hepatocellular carcinoma. *Liver Res*. 2022;6:258–268. https://doi.org/10.1016/j.livres.2022.12.002.
4. Makarova-Rusher OV, Medina-Echeverz J, Duffy AG, Greten TF. The yin and yang of evasion and immune activation in HCC. *J Hepatol*. 2015;62:1420–1429. https://doi.org/10.1016/j.jhep.2015.02.038.
5. Shlomai A, de Jong YP, Rice CM. Virus associated malignancies: the role of viral hepatitis in hepatocellular carcinoma. *Semin Cancer Biol*. 2014;26:78–88. https://doi.org/10.1016/j.semcancer.2014.01.004.
6. Landskron G, De la Fuente M, Thuwajit P, Thuwajit C, Hermoso MA. Chronic inflammation and cytokines in the tumor microenvironment. *J Immunol Res*. 2014;2014:149185. https://doi.org/10.1155/2014/149185.
7. Galun E. Liver inflammation and cancer: the role of tissue microenvironment in generating the tumor-promoting niche (TPN) in the development of hepatocellular carcinoma. *Hepatology*. 2016;63:354–356. https://doi.org/10.1002/hep.28344.
8. Ray K. Liver cancer: a complex interplay between inflammation and immunity in liver cancer. *Nat Rev Gastroenterol Hepatol*. 2018;15:3. https://doi.org/10.1038/nrgastro.2017.165.
9. Chew V, Chen J, Lee D, et al. Chemokine-driven lymphocyte infiltration: an early intratumoural event determining long-term survival in resectable hepatocellular carcinoma. *Gut*. 2012;61:427–438. https://doi.org/10.1136/gutjnl-2011-300509.
10. Chew V, Tow C, Teo M, et al. Inflammatory tumour microenvironment is associated with superior survival in hepatocellular carcinoma patients. *J Hepatol*. 2010;52:370–379. https://doi.org/10.1016/j.jhep.2009.07.013.
11. Hou J, Zhang H, Sun B, Karin M. The immunobiology of hepatocellular carcinoma in humans and mice: basic concepts and therapeutic implications. *J Hepatol*. 2020;72:167–182. https://doi.org/10.1016/j.jhep.2019.08.014.
12. Garnelo M, Tan A, Her Z, et al. Interaction between tumour-infiltrating B cells and T cells controls the progression of hepatocellular carcinoma. *Gut*. 2017;66:342–351. https://doi.org/10.1136/gutjnl-2015-310814.
13. Zhang L, Qin Q, Xu C, Zhang N, Zhao T. Identification of immune cell function in breast cancer by integrating multiple single-cell data. *Front Immunol*. 2022;13:1058239. https://doi.org/10.3389/fimmu.2022.1058239.
14. Guan MC, Wang MD, Wang WY, et al. Exosomes as mediators of tumor immune escape and immunotherapy in hepatocellular carcinoma. *Liver Res*. 2022;6:132–138. https://doi.org/10.1016/j.livres.2022.08.001.
15. Lopez JS, Banerji U. Combine and conquer: challenges for targeted therapy combinations in early phase trials. *Nat Rev Clin Oncol*. 2017;14:57–66. https://doi.org/10.1038/nrclinonc.2016.96.
16. Liu X, Xia F, Chen Y, et al. Chinese expert consensus on refined diagnosis, treatment, and management of advanced primary liver cancer (2023 edition). *Liver Res*. 2024;8:61–71. https://doi.org/10.1016/j.livres.2024.05.001.
17. Kotsari M, Dimopoulou V, Koskinas J, Armakolas A. Immune system and hepatocellular carcinoma (HCC): new insights into HCC progression. *Int J Mol Sci*. 2023;24:11471. https://doi.org/10.3390/ijms241411471.
18. Zhang Q, He Y, Luo N, et al. Landscape and dynamics of single immune cells in hepatocellular carcinoma. *Cell*. 2019;179:829–845 (e20). https://doi.org/10.1016/j.cell.2019.10.003.
19. Zhu C, Xiao H, Jiang X, Tong R, Guan J. Prognostic biomarker DDOST and its correlation with immune infiltrates in hepatocellular carcinoma. *Front Genet*. 2022;12:819520. https://doi.org/10.3389/fgene.2021.819520.
20. Tu Z, Ji Q, Han Q, et al. Intrinsic immune evasion patterns predict temozolomide sensitivity and immunotherapy response in lower-grade gliomas. *BMC Cancer*. 2022;22:973. https://doi.org/10.1186/s12885-022-09984-5.
21. Kanehisa M, Goto S. KEGG: kyoto encyclopedia of genes and genomes. *Nucleic Acids Res*. 2000;28:27–30. https://doi.org/10.1093/nar/28.1.27.
22. Han Y, Wang Y, Dong X, et al. TISCH2: expanded datasets and new tools for single-cell transcriptome analyses of the tumor microenvironment. *Nucleic Acids Res*. 2023;51:D1425–D1431. https://doi.org/10.1093/nar/gkac959.
23. Marderstein AR, Uppal M, Verma A, et al. Demographic and genetic factors influence the abundance of infiltrating immune cells in human tissues. *Nat Commun*. 2020;11:2213. https://doi.org/10.1038/s41467-020-16097-9.
24. Chen B, Khodadoust MS, Liu CL, Newman AM, Alizadeh AA. Profiling tumor infiltrating immune cells with CIBERSORT. *Methods Mol Biol*. 2018;1711:243–259. https://doi.org/10.1007/978-1-4939-7493-1_12.
25. Hänzelmann S, Castelo R, Guinney J. GSVA: gene set variation analysis for microarray and RNA-seq data. *BMC Bioinformatics*. 2013;14:7. https://doi.org/10.1186/1471-2105-14-7.
26. Xu L, Deng C, Pang B, et al. TIP: a web server for resolving tumor immunophenotype profiling. *Cancer Res*. 2018;78:6575–6580. https://doi.org/10.1158/0008-5472.CAN-18-0689.
27. Robin X, Turck N, Hainard A, et al. pROC: an open-source package for R and S+ to analyze and compare ROC curves. *BMC Bioinformatics*. 2011;12:77. https://doi.org/10.1186/1471-2105-12-77.
28. Yu S, Wang G, Shi Y, Xu H, Zheng Y, Chen Y. MCMs in cancer: prognostic potential and mechanisms. *Anal Cell Pathol (Amst)*. 2020;2020:3750294. https://doi.org/10.1155/2020/3750294.
29. Cai C, Zhang Y, Hu X, et al. CDT1 is a novel prognostic and predictive biomarkers for hepatocellular carcinoma. *Front Oncol*. 2021;11:721644. https://doi.org/10.3389/fonc.2021.721644.
30. He Y, Wu Y, Song M, Yang Y, Yu Y, Xu S. Establishment and validation of a ferroptosis-related prognostic signature for hepatocellular carcinoma. *Front Oncol*. 2023;13:1149370. https://doi.org/10.3389/fonc.2023.1149370.
31. Sripathi SR, Hu MW, Turaga RC, et al. IKKβ inhibition attenuates epithelial mesenchymal transition of human stem cell-derived retinal pigment epithelium. *Cells*. 2023;12:1155. https://doi.org/10.3390/cells12081155.
32. Reicherz A, Eltit F, Scotland K, et al. Indwelling stents cause severe inflammation and fibrosis of the ureter via urothelial-mesenchymal transition. *Sci Rep*. 2023;13:5492. https://doi.org/10.1038/s41598-023-31885-1.
33. Shi P, Xu J, Cui H. The recent research progress of NF-κB signaling on the proliferation, migration, invasion, immune escape and drug resistance of glioblastoma. *Int J Mol Sci*. 2023;24:10337. https://doi.org/10.3390/ijms241210337.
34. Sokratous G, Polyzoidis S, Ashkan K. Immune infiltration of tumor microenvironment following immunotherapy for glioblastoma multiforme. *Hum Vaccin Immunother*. 2017;13:2575–2582. https://doi.org/10.1080/21645515.2017.1303582.